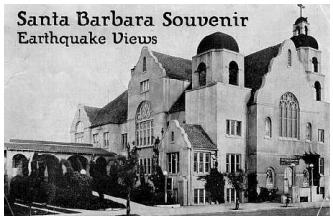

4th IASPEI / IAEE International Symposium:

Effects of Surface Geology on Seismic Motion

August 23–26, 2011 · University of California Santa Barbara

NEAR-SOURCE GROUND MOTION VARIABILITY FROM M~6.5 DYNAMIC RUPTURE SIMULATIONS

Luis A. DALGUER
Swiss Seismological Service, ETH-Zurich
Zurich, CH-8092
Switzerland

P. Martin MAI
Division of Physical Sciences and Engineering KAUST
Thuwal, 23955-6900
Saudi Arabia

ABSTRACT

We study ground-motion variability from dynamic rupture simulations, with a particular focus on PGA-values exceeding 1g in moderate earthquakes. Such extreme ground motions are generally observed near the ruptured fault, and it is expected that they are dominated by source effects. We investigate earthquake source characteristics and near-source ground motion using spontaneous dynamic rupture simulations of earthquakes of ~M 6.5. We generate a large number of dynamic source models with stochastic initial stress distribution for three classes of faulting (thrust, normal and strike slip) with buried and surface rupturing faults. Stress and frictional strength consider two extreme cases of normal stress, 1) depth-dependent, and 2) depth-independent. This diversity of rupture models generates a broad range of scenarios for evaluating near-source ground motion variability and for identifying the causes for extreme ground motion. Comparing PGV and PSA of our simulation with empirical GMPE, we find an increased variability in the near-field of the rupture. The consistent saturation of these quantities predicted by GMPE is not obvious in our calculations. Rather, there are significant ground-motion reductions near the source for buried faults, but considerable increase for surface rupturing earthquakes. Extreme ground motions appear to be correlated with faulting that breaks the free surface, with largest shaking levels for strike-slip ruptures. For buried ruptures, thrust faulting earthquakes generate the strongest ground motion, normal faulting the weakest. In general, simulated ground motion are consistent with GMPE's at distance >5km, but not at short distance.

INTRODUCTION

Earthquake numerical models based on physics of the causative rupture and wave propagation, that incorporate conservation laws of continuum mechanics, frictional sliding, and the state of stress in the crust, have expanded our understanding of both source- and propagation-dominated ground motion phenomena (e.g., Dunham and Archuleta, 2005; Dalguer et al, 2008; Dunham and Bhat, 2008; Olsen et al, 2009). In these models the fault kinematics (slip and slip rate) and rupture propagation are determined dynamically as part of the solution of the problem, by solving, the elastodynamic equation coupled to frictional siding. They usually idealize the earthquake rupture as a propagating shear crack on a frictional interface embedded in a linearly elastic continuum. This idealization has proven to be a useful foundation for analyzing and simulating natural earthquakes (e.g., Andrews, 1976; Das and Aki, 1977; Day, 1982a,b; Olsen et al., 1997; Oglesby et al., 1998; Dalguer et al., 2001; Peyrat et al., 2001; Day et al., 2008), and we adopt it here. The use of these dynamic rupture models to simulate earthquakes is gaining increasing importance in the Earth science and earthquake engineering community, because these models allows us to deal more closely with the physical processes that determine an earthquake and have greater potential to capture details of the physical rupture process and near-source ground motion variability. Understanding these aspects improve our capability to predict near-source ground motion, and therefore allows a more accurate assessment of the seismic hazard and risk.

It is well known that current empirical ground motion prediction equations (GMPE) are insufficient for the prediction of near-source ground motion for use in seismic hazard and risk assessment. That is because these GMPE are based solely on recorded data which are sparse in the near field, and which do not adequately represent the source effects and the geologic amplification mechanisms that have been identified in numerical simulations. Therefore, physics-based numerical models are required if we are to adequately assess the level and variability of near-source ground motion, for events consistent with the maximum expected earthquake in the zone of study.

Modern dense near-source seismic recording of recent earthquakes have revealed that acceleration ground motion exceeding 1g appears to be often in moderate shallow earthquakes (e.g. 2008 M_w 6.9 Iwate-Miyagi Nairiku, Japan; 2010 M_w7.0 Darfield, New Zealand; 2011 M_w 6.3 Christchurch, New Zealand) in frequency range of engineering interest (1.0 – 10.0 Hz). In particular, the recorded ground motion exceeding 1g at relatively low frequency of ~1.0Hz during the 2011 M_w 6.3 Christchurch event is even more surprising, and can be extremely damaging for tall buildings.

Here we use dynamic rupture models to examine ground motion characteristics for three classes of faulting (thrust, normal and strike slip) for buried and surface earthquakes. Stress and frictional strength consider two extreme cases of normal stress, 1) depth-dependent, and 2) depth-independent. Our simulations are tailored to assemble a set of 30 M_w ~6.5 scenario earthquakes for each faulting style and each case (buried and surface faulting with depth and non-depth normal stress dependent) with a total of 360 simulations. The resulting ground motions are compared with empirical predictions equations. Models predicting acceleration exciding 1g are evaluated with appropriate recent near-field observations.

Calculations are developed using the Support Operator Rupture Dynamics code (SORD). The SORD code (Ely et al., 2008, 2009) is based on a generalized Finite Difference scheme that can utilize meshes of arbitrary structure and incorporate irregular geometry, with the capability to model general fault geometry and topography. The dynamic rupture occurs as dictated by the local stress conditions and follow the slip-weakening friction model in the form given Andrews (1976). The code is parallelized, using Message Passing Interface (MPI), for multiprocessor execution, and is highly scalable, enabling large-scale earthquake simulations. The dynamic rupture model has been validated through the Southern California Earthquake Centre (SCEC) dynamic rupture code validation exercise, showing good agreement with semi-analytical boundary integral methods (Harris et al., 2009).

DYNAMIC RUPTURE MODEL PARAMETERIZATION METHODOLOGY

The assumption of initial stress and frictional strength prior to earthquake are fundamental for realistic simulation of earthquakes in nature. Assuming that shear failure on pre-existing faults of shallow earthquakes is governed by Coulomb friction, the mode of faulting and the loading history in compressional and extensional tectonic regimes play an important role in determining the initial stress and the absolute value of frictional strength on the fault (e.g. Sibson, 1991). Considering for example a fault system under confining pressure equivalent to the gravitational load, the tectonic loading in a compressional regime accumulates shear stress on the fault while simultaneously frictional strength is expected to increase due to increasing normal stress. In contrast, tectonic loading in an extensional regime results in a reduction of the shear strength due to decreasing normal stress .

Normal Stress Depth Dependent Model. Stress parameterization follow the methodology proposed by Dalguer and Mai (2008) to estimate the strength and initial stress on the fault prior to rupture. Their approach combines stochastic initial stress fields with a realistic fault-loading environment in which the tectonic loading regime (compressional or extensional) and the gravitational loading determine the absolute value of fault frictional resistance and initial stress. The procedure is as follows:

1) Assume that far-field stress is initially equal to the confining pressure, which is equivalent to the gravitational load

$$\sigma_1=\sigma_2=\sigma_3=\rho g h \tag{1}$$

where $\boldsymbol{\sigma_1}$, $\boldsymbol{\sigma_2}$ and $\boldsymbol{\sigma_3}$, are respectively the principal stresses, ρ the density, g the acceleration of gravity and h the depth

2) Loading of principal stresses. Increase σ_1 for thrust or strike-slip faulting; or decrease σ_3 for normal faulting events; this represents a "loading" or stress-increasing mechanism for thrust/strike-slip events, and an "unloading" or stress-reduction mechanism for normal faults.

$$\begin{aligned} \sigma_1 &= \rho g h + \Delta\sigma_{load} \quad \text{loading} \\ \sigma_3 &= \rho g h + \Delta\sigma_{load} \quad \text{unloading} \end{aligned} \tag{2}$$

where $\Delta\boldsymbol{\sigma_{load}}$ is the stress increment/decrement to load/unload the system

3) Estimate the normal stress acting on a specific fault plane from the loaded/unloaded principal stresses, using

$$\sigma_n = \frac{1}{2}(\sigma_1+\sigma_3) + \frac{1}{2}(\sigma_1-\sigma_3)\cos(\theta) \tag{3}$$

where θ is the fault plane angle measured with the σ_3 axes .

4) Estimate the frictional strength (assuming Coulomb friction), based on

$$\tau_c = c + \mu_f(\sigma_n - p) \tag{4}$$

where c is cohesion stress, p is pore pressure (here: hydrostatic pressure), then $(\sigma\text{-}p)$ is the effective normal stress, and μ_f is the friction coefficient that depends on slip (slip weakening model) in the form given by Andrews (1976) as follow

$$\mu_f = \begin{cases} \mu_s - (\mu_s - \mu_d)u/d_0 & u < d_0 \\ \mu_d & u \geq d_0 \end{cases} \tag{5}$$

where μ_s and μ_d are respectively the static and dynamic friction coefficient, u the slip and d_0 the critical slip distance.

5) Estimate initial shear stress on the fault as

$$\tau_0 = \tau_{st} + \Delta\tau_{ld} \tag{6}$$

where τ_{st} is a heterogeneous stress field (Ripperger et al., 2007, 2008) generated as a spatial random field that represents the remaining stress from the history of previous events. This stochastic stress is first tapered in an arbitrary non-depth dependent frictional strength profile such that its maximum (τ_{max}) is close to the static failure stress (τ_s) and its minimum (τ_{min}) is the final stress from the last past earthquake characterized with the dynamic overshoot ($k_{osd} > 1$) or undershoot ($k_{osd} < 1$) coefficient.

$$\tau_{\mathbf{max}} = \tau_s; \qquad \tau_{\mathbf{min}} = \tau_s - (\tau_s - \tau_d)k_{osd} \tag{7}$$

Finally, the τ_{st} is again tapered to the depth dependent frictional strength profile calculated in Step 4, but keeping the same ratio $(\tau_0\text{-}\tau_d)/(\tau_s\text{-}\tau_d)$, where $\boldsymbol{\tau_s}$ and $\boldsymbol{\tau_d}$ are respectively the static and dynamic frictional strength. $\Delta\tau_{ld}$ in Equation 6 is a small stress increment for additional loading in the nucleation zone in order to initiate rupture instability (Ripperger et al 2007, 2008).

6) Determine the size of the nucleation zone, a circular patch with radius L_c, half of the critical length of an equivalent uniform fault with initial stress and frictional strength corresponding to the average over the fault. L_c has the form (e.g, Day et al, 2005):

$$L_c = \frac{\mu d_0(\tau_{bav})}{\pi(\Delta\tau_{av})^2} + \Delta\tau_{ld} \tag{8}$$

where μ is the shear modulus and τ_{bav} and $\Delta\tau_{av}$ are respectively the average breakdown strength drop and average stress drop. Depending on the stress parameterization, L_c may take on large values. Because large nucleation regions would influence the dynamic rupture properties over a large fault area, it is necessary to choose L_c as small as possible. Our numerical experiment shows that with L_c = 2.0 km is often enough to trigger rupture, so we assumed a maximum L_c of 2.0 km. The center of the nucleation zone is given stochastically, defined as the point in which the initial stress is equal to the yielding stress, as defined in step (5).

7) Shallow part, brittle crust and ductile zone. As shown in Figure 1, our parameterization considers stable zone (shallow part), brittle crust (seismogenic zone) and ductile zone (deepest layer). The normal stress depth dependent parameterization produces a weak zone in the shallow depth unable to maintain large shear stress. If this shallow depth is not parameterized in an appropriate way, early and unrealistic rupture process may take place in this zone. In addition, some studies (e.g. Brune and Anooshehpoor, 1998; Day and Ely, 2002) suggest that rupture at this weak shallow zone should operate in a distinctive manner from the rest of the fault, such as strength hardening due to the formation of incompetent fault gouge, cracking (e.g. Marone, 1998; Marone and Scholz, 1988), or due to the presence of thick surface deposits of sediments, fissured rocks and other forms of off-fault zone damage. The main feature of this shallow depth zone is that it operates during rupture with an enhanced energy absorption mechanism. We define the first 2 km depth as a weak shallow zone, which obeys to strength hardening during frictional sliding. To model this frictional behavior, we assume negative stress drop and large critical slip distance in this zone, defined as the stable uppermost layer (Figure 1). The seismogenic zone, below the stable zone, represents the brittle crust of the earth. We model it as an 18 km thick layer. Below this seismogenic layer, we considered a ductile zone, characterized by large critical slip distance (Figure 1). Rupture may propagate dynamically into the weak shallow layer or into the deep ductile zone, but they cannot nucleate in these regions. Once the dynamic rupture has entered these zones, it is likely to terminate soon as the energy-absorption at the crack tip exceeds the energy supplied by the propagating crack.

Normal Stress Non-depth Dependent Model. The stress parameterization for this case follows the same procedure as described above, with the difference that the normal stress acting on the fault is constant over the fault.

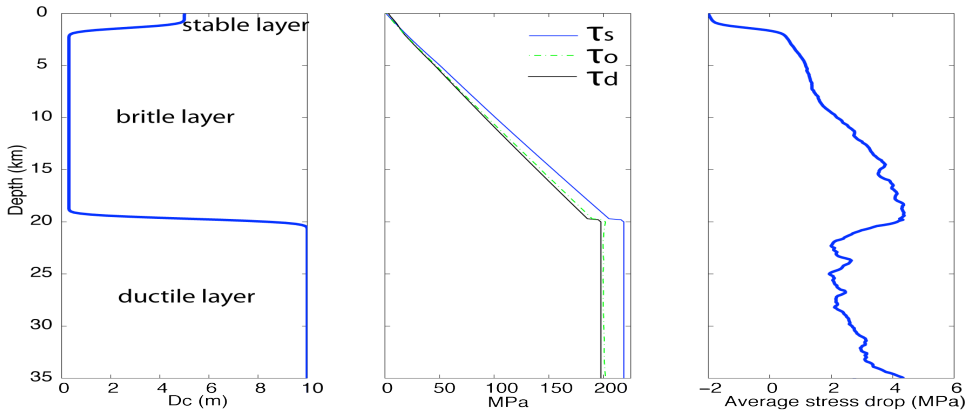

Figure 1. An example of depth variation of frictional parameters averaged along the strike of the fault, adopted in the dynamic rupture models. Left figure shows critical slip distance. Center shows the static frictional strength (τ_s), initial stress (τ_0) and dynamic frictional strength (τ_d). Right figure shows the stress drop.

MODEL PARAMETRIZATION

The list below summarizes the modeling parameters adopted in our dynamic rupture simulations:

- Strike-slip faulting: dip=90° fault length = 30km fault width=12km
- Thrust faulting: dip=45° fault length = 24km fault width=15km
- Normal faulting dip=60° fault length = 24km fault width=15km
- For ruptures that are not allowed to break the surface, the faults are buried at 5km depth
- Static friction coefficient = 0.6 dynamic friction coefficient = 0.56 cohesion force = 1.0×10e6 Pa;
- dynamic overshoot coefficient = 1.5 critical slip distance = 0.2
- critical slip distance smoothly increases from 0.3 m to 5 m at fault boundaries in a 3 km-wide buffer zone that surrounds the above defined fault areas; this approach ensures that rupture propagation stops smoothly at the borders of the fault
- loading under compression (trust/ strike slip fault), unloading under extension (normal fault) = 50×10e6 Pa. The loading is applied at 15km depth.
- strike-slip faults have the principal stress σ_2 equal to the average between σ_1 and σ_3, and the angle θ of equation 2 is 45° (fault plane angle measured with the σ_3 axes)
- initial stress stochastic field realizations based on von Karman distribution with correlation length of 8.0 km in along-strike and along-dip direction, Hurst number H = [0, 0.25, 0.5]; resulting stress distribution are hence compatible to seismological observations (Mai and Beroza, 2002).
- normal stress = 120 MPa, for model with non-depth dependent stress
- layered 1D velocity-density structure, derived as the average model of available models in Switzerland (Figure 2)
- numerical setup uses 8 grid element per wavelength; a conservative estimate yields that we accurately resolve a maximum frequency of ~3 Hz, given the chosen velocity structure and grid size of 100 m; domain-size 100 km x 100 km x 30 km
- simulations were carried out on "Rosa", a Cray XT5 at the Swiss National Supercomputing Center (CSCS), on 4096 CPUs

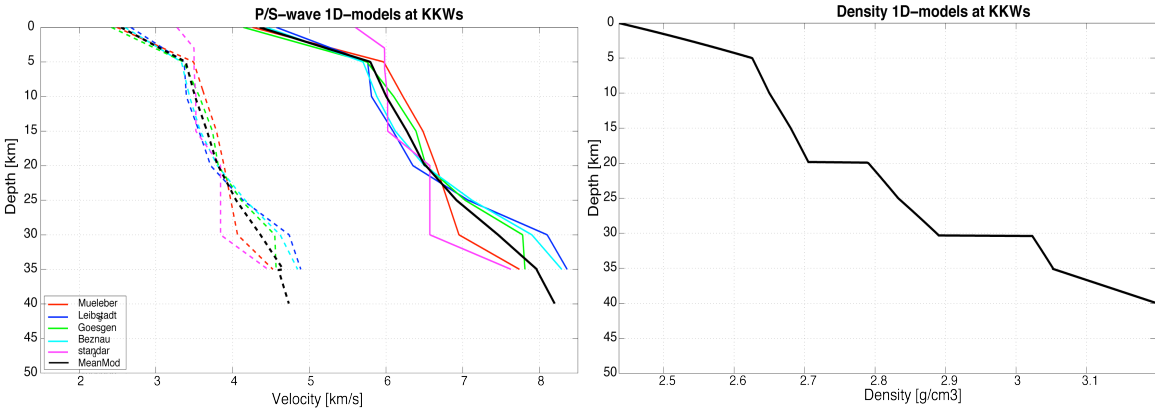

Figure2. 1D velocity structure model (left) and density (right) used for dynamic rupture simulations.

NUMERICAL RESULTS

Dynamic Rupture Solutions. From the total of 360 models, that include buried and surface rupture with normal stress depth and non dependent models for three classes of faulting (strike, reverse and normal-slip), a diversity of rupture scenarios has been simulated in a range of M_w 5.5 – 7.0. Figures 3, 4 and 5 show respectively for strike, reverse and normal-slip fault, representative models with the same stochastic stress parameterization for each type of rupture. The rupture propagation, slip, peak slip velocity and stress drop distribution evolve in a diverse manner within the three class of faulting. For each case of rupture (buried and surface-rupturing) models with non-depth dependent stress parameterization results in solutions with larger stress drop, but earthquake size is larger for depth dependent stress models. Surface rupturing model with depth dependent stress predict the largest size earthquake, but the non-dependent stress model results in the largest peak slip rate values.

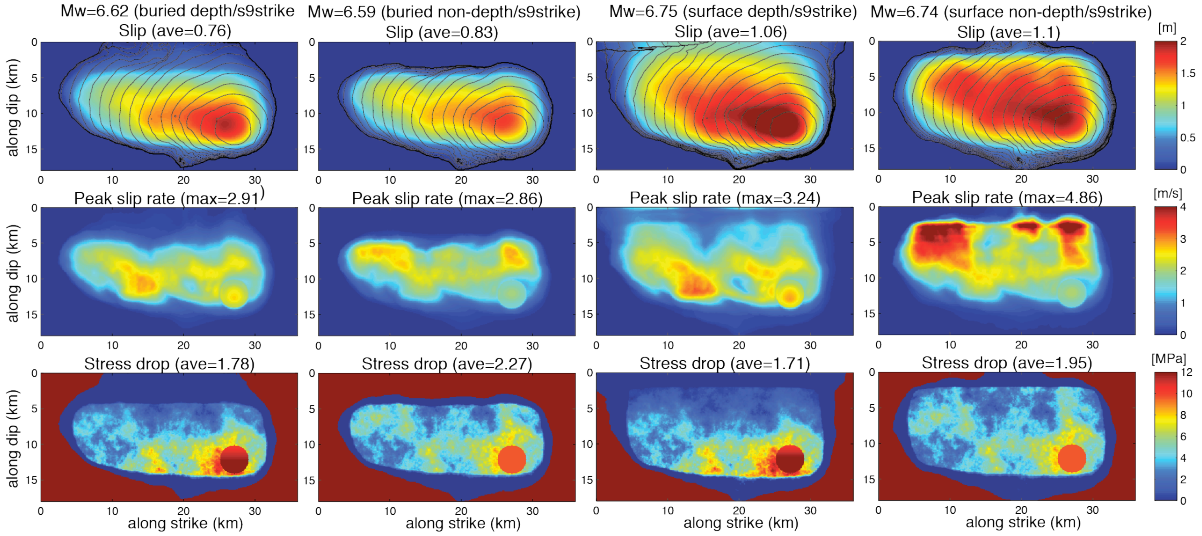

Figure 3. Dynamic rupture solutions for a strike-slip rupture with the identical stochastic stress parameterization, for depth and non-depth dependent stress and for buried and surface-rupturing models. Top shows slip distribution, contour line is the rupture time each 0.5 sec. Center shows peak-slip distribution, and bottom is stress drop distribution.

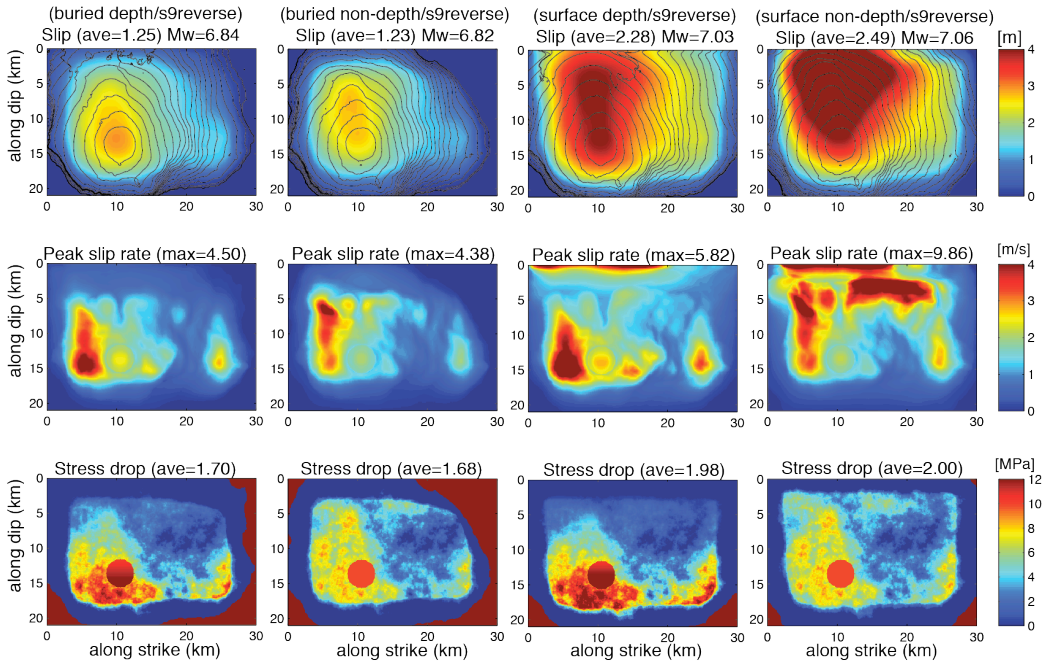

Figure 4. Dynamic rupture solutions for reverse-slip rupture with the identical stochastic stress parameterization, for depth and non-depth dependent stress and for buried and surface-rupturing models. See Figure 3 for details.

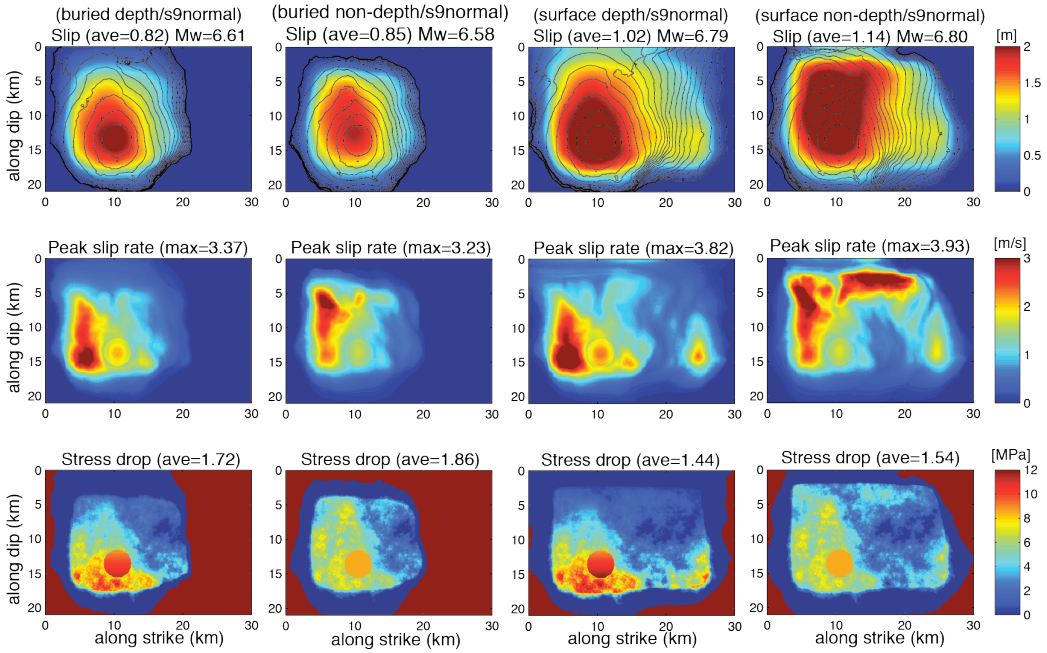

Figure 5. Dynamic rupture solutions for a normal-slip rupture with the identical stochastic stress parameterization, for depth and non-depth dependent stress and for buried and surface-rupturing models. See Figure 3 for details.

Ground Motion Solutions.

We compare the resulting ground motions of all 360 models to common ground-motion prediction equations (GMPE) and observations, focusing on the maximum ground motion generated by these models. Site-amplification corrections using the period-dependent amplification coefficient of Borcherdt (1994, 2002) are applied to scale computed ground motions to Vs30=1500m/s from the minimum shear-wave velocity in our simulations (Vs30=2500m/s). This correction is needed to facilitate the comparison with the GMPE's that are based on Vs30-values less than 1500 m/s. Synthetic ground motions are filtered using a band pass Butterworth filter from 0.01 to 3.0 Hz. Figure 6 displays PGV and PGA (for wave forms up to f_{max} = 3 Hz) for all models. We find that surface rupturing models predict stronger ground motion than buried rupture, with the strongest corresponding to non-depth dependent stress models, acceleration exceeding in some case gravity. Strike slip models predict the strongest ground motion, followed by reverse-slip rupture models. Maximum ground motion levels is constant up to M_w~6.3 for strike slip fault, and up to M_w~6.7 for reverse and normal faults. Differences in ground-motions between buried ruptures with depth and non-depth dependent stress are indistinguishable.

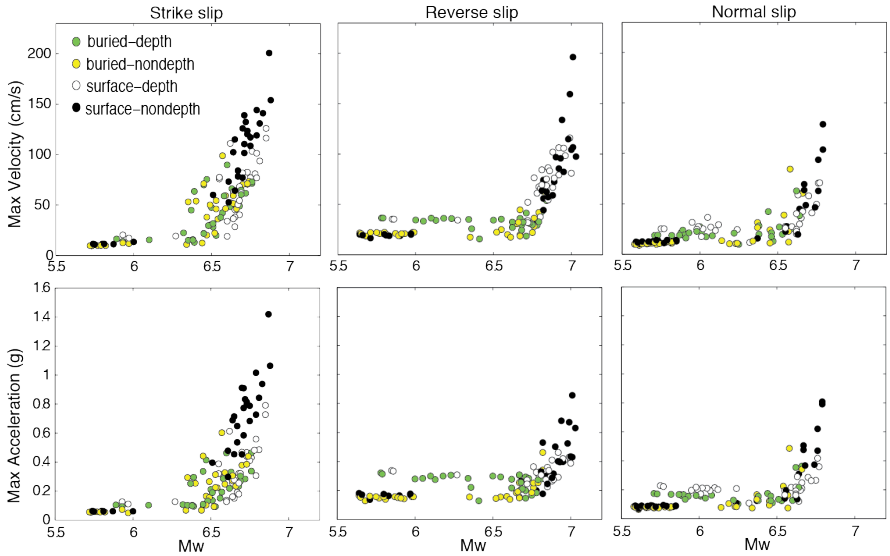

Figure 6. Maximum horizontal ground motion of velocity (top) and acceleration (bottom) for strike, reverse and normal faults of buried and surface rupturing with depth and non-depth dependent stress for a total of 360 models.

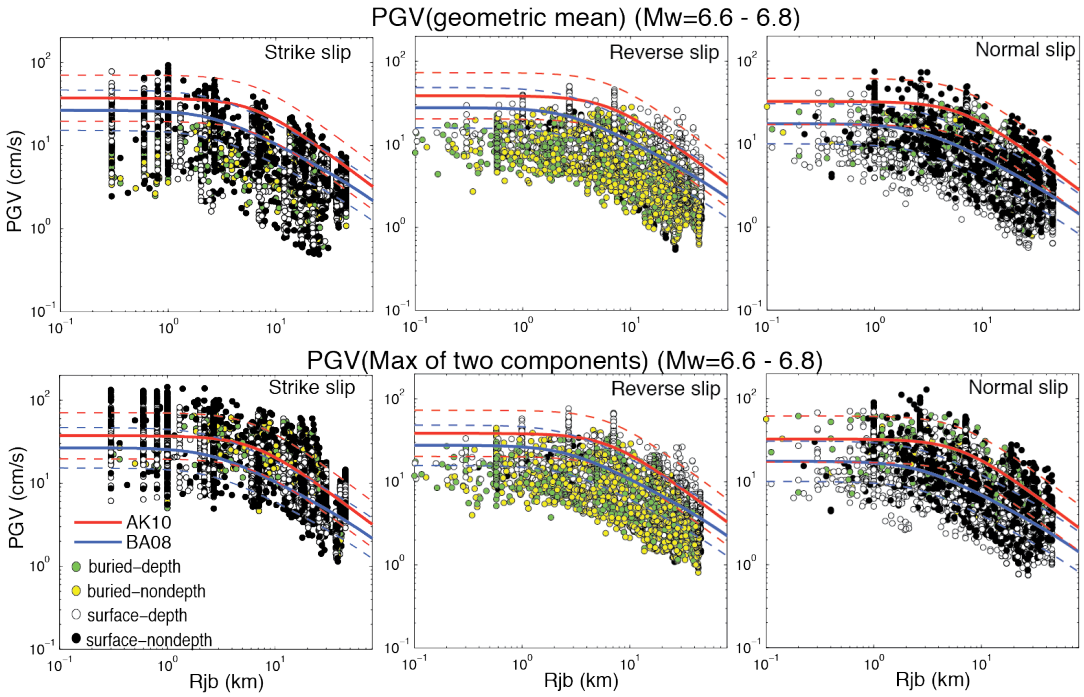

Figure 7. Horizontal PGV comparisons with GMPE from AK10 (Akkar and Bommer, 2010) and BA08 (Boore and Atkinson, 2008) and for strike, reverse and normal faults of buried and surface rupturing with depth and non-depth dependent stress, for models in the magnitude range M_w 6.6 – 6.8. Top shows comparison using the classic geometric and bottom correspond to the maximum of the two horizontal components.

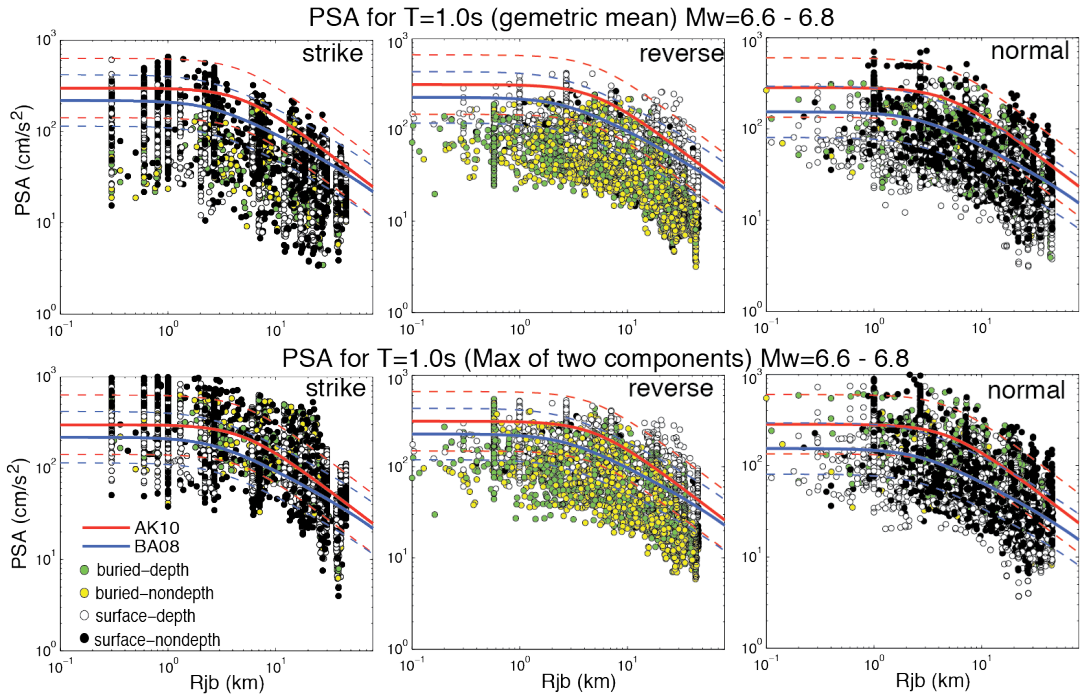

Figure 8. Horizontal Pseudo Spectral Acceleration (PSA) at period T=1.0s compared with GMPE of AK10 (Akkar and Bommer, 2010) and BA08 (Boore and Atkinson, 2008) for strike, reverse and normal faults of buried and surface rupturing with depth and non-depth dependent stress, for models in the magnitude range M_w 6.6 – 6.8. Top shows comparison using the classic geometric and bottom correspond to the maximum of the two horizontal components.

Figures 7 and 8 compare, respectively, PGV and PSA (at period T=1.0s) with GMPE from Akkar and Bommer (2010) hereafter AK10 and Boore and Atkinson (2008) here after BA08, for a range of magnitude of M_w 6.6 – 6.8. We use Joyner-Boore Distance (R_{jb}). The PGV and PSA estimate from our simulations are calculated assuming two criteria, the geometric mean of the two maximum horizontal components (top of Figure 7,8) and the maximum value of the two maximum horizontal components (bottom of Figure 7, 8). In general PGV and PSA are consistent with GMPE, with better fitting at distance R_{jb} larger than about 3-7 km than at very close distances to the fault. Estimates using the maximum criterion provide better comparison than the geometric mean criterion. We find an increased variability in the near-field of the rupture. The consistent saturation of these quantities as predicted by GMPE is not obvious in our calculations. Rather, there are significant ground-motion reductions near the source for buried faults and for dip-slip ruptures, but considerable increase for strike slip surface rupturing earthquakes.

Extreme ground motion appears to be correlated with faulting that breaks the free-surface with the strongest for strike-slip rupture, predicting acceleration ground motion exceeding the gravity. Figure 9a shows a representative of PSA exceeding the gravity predicted by surface rupturing of strike, reverse and normal-faulting models with non-depth dependent normal stress. As seen in this figure, gravity is exceeded at frequencies in the range of 1.0 – 2.5 Hz (T = 0.4 – 1.0s). For reference, Figure 9b displays PSA at several stations exceeding gravity during the 2011 M_w 6.3 Christchurch, New Zealand earthquake, in which extreme ground motion were observed in the same frequency range.

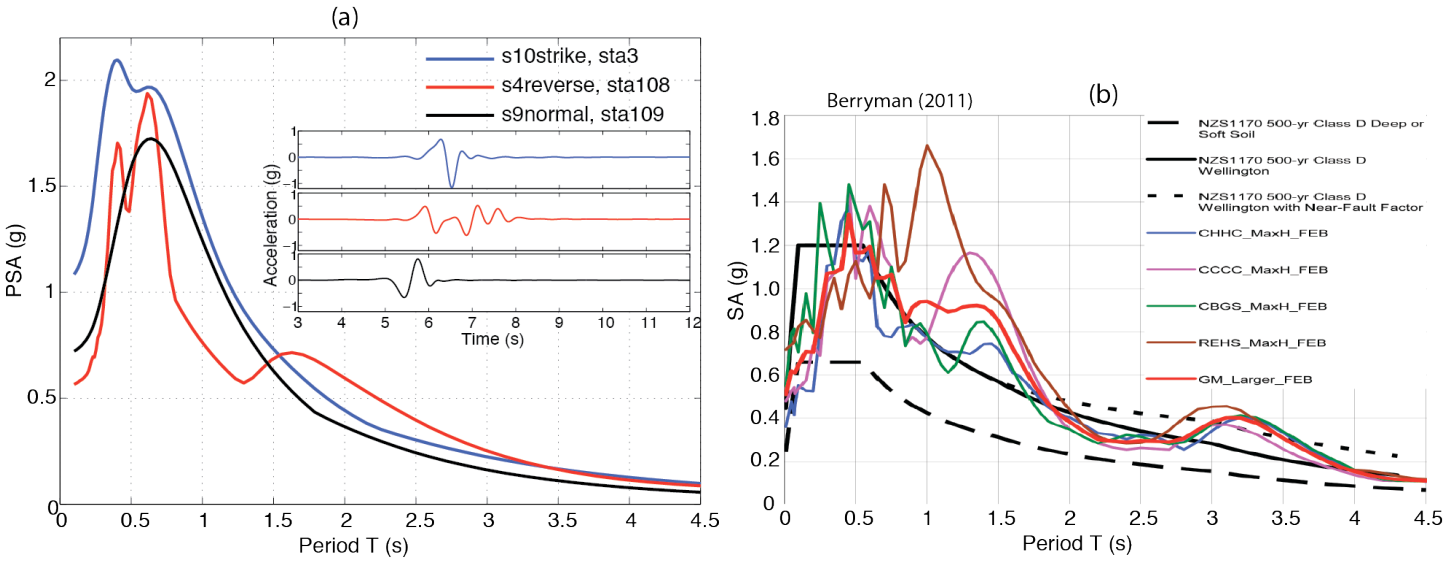

Figure 9. Left (a) PSA at selected station very near the source for strike, reverse and normal faulting with surface rupturing and non-depth dependent stress; the inset figure displays the corresponding acceleration time histories. Right (b), Spectral Acceleration at several stations exceeding gravity during the 2011 M_w 6.3 Christchurch, New Zealand earthquake (After Berryman, 2011). Solid and dashed black line are design spectral motions.

CONCLUSIONS

We have developed suite of rupture dynamic simulation to evaluate ground-motion variability generated by those events, with a particular focus on extreme ground motion acceleration exceeding 1g in earthquake in the range of M_w ~5.5 –7.0. A total of 360 source models for strike, reverse and normal faulting with buried and surface rupturing features as well as depth and non-depth dependent stress parameterization have been generated and their resulting near-field ground-motions examined. This diversity of rupture models creates a broad range of scenarios for evaluating near-source ground motion variability and for identifying the causes for extreme ground motion. Surface rupturing events predict the stronger ground motion than buried rupture, with the strongest for surface rupturing models with non-depth dependent stress. In general, simulated ground motion are consistent with GMPE's at distance >5km, but not at short distance. The consistent saturation very near the source of ground motion quantities as predicted by GMPE is not obvious in our calculations, rather, there are significant ground-motion reductions near the source, particularly for buried faults, and considerable variability for surface rupturing earthquakes. There is an increased variability in the near-field considering all the rupture models. Extreme ground motion appear to be correlated with faulting that breaks the free-surface with the strongest for strike-slip rupture. We found ground motion at some stations very near to the source that exceed the gravity acceleration at frequencies range 1.0 to 2.5Hz, those extreme ground motions resemble the ground motion recorded during the 2011 M_w 6.3 Christchurch, New Zealand earthquake that occurs at such as frequency range.

REFERENCES

Akkar, S and J. Bommer, 'Empirical equations for prediction of PGA, PGV, spectral accelerations in Europe, the Mediterranean region and the Middle East', SRL, in press.

Andrews, D.J (1976). Rupture velocity of plane-strain shear cracks, J. Geophys. Res., 81, 5679-5687.

Andrews, D. J. (1999). Test of two methods for faulting in finite-difference calculations, Bull. Seism. Soc. Am. 89, 931–937.

Berryman, K (2011), A tale of two earthquakes – the Christchurch sequence of 2010-2011, Proc. G-Ever1 Conference, Tsukuba, march 2011.

Boore, D. M., and G. M. Atkinson (2008). Ground-motion prediction equations for the average horizontal component of PGA, PGV, and 5%-damped PSA at spectral periods between 0.01 s and 10.0 s, Earthquake Spectra 24, 99–138

Borcherdt RD (1994) Estimates of site-dependent response spectra for design (methodology and justification). Earthquake Spectra 10(4):617–653

Borcherdt RD (2002) Empirical evidence for acceleration-dependent amplification factors. Bull. Seis Soc Am. 92(2):761–782

Dalguer L.A; Irikura K; Riera J. And Chiu H.C (2001). The Importance of the Dynamic Source Effects on Strong Ground Motion During the 1999 Chi-Chi (Taiwan) Earthquake: Brief Interpretation of the Damage Distribution on Buildings. Bull. Seismol. Soc. Am., 95, 1112-1127.

Dalguer, L. A. and Day, S. M. (2007), Staggered-Grid Split-Nodes Method for Spontaneous Rupture Simulation. J. Geophys. Res., 112, B02302, doi:10.1029/2006JB004467.

Dalguer, L.A., H. Miyake, S.M. Day and K. Irikura (2008), Surface Rupturing and Buried Dynamic Rupture Models Calibrated with Statistical Observations of Past Earthquakes. Bull. Seismol. Soc. Am. 98, 1147-1161, doi: 10.1785/0120070134.

Dalguer, L.A. and M. Mai (2008), Implications of Style-of-Faulting and Loading Characteristics on the Dynamic Rupture Process, Eos Trans. AGU, 89(53), Fall Meet. Suppl., Abstract S51D-1798

Das, S., and K. Aki (1977). Fault planes with barriers: A versatile earthquake model, J. Geophys. Res., 82, 5648-5670.

Day, S. M. (1982a). Three-dimensional finite difference simulation of fault dynamics: rectangular faults with fixed rupture velocity, Bull. Seismol. Soc. Am., 72, 705-727.

Day, S. M. (1982b). Three-dimensional simulation of spontaneous rupture: the effect of nonuniform prestress, Bull. Seismol. Soc. Am., 72, 1881-1902.

Day, S. M., L. A. Dalguer, N. Lapusta, and Y. Liu (2005), Comparison of finite difference and boundary integral solutions to three-dimensional spontaneous rupture, J. Geophys. Res., 110, B12307, doi:10.1029/2005JB003813.

Day, S. M., S. H. Gonzalez, R. Anooshehpoor, and J. N. Brune (2008). Scale-model and numerical simulations of near-fault seismic directivity, Bull. Seism. Soc. Am. , Vol. 98, doi: 10.1785/0120070190, pp. 1186-1206

Dunham, E., and R. Archuleta (2005). Near-source ground motion from steady state dynamic rupture pulses, Geophys. Res. Lett. 32, L03302, doi:10.1029/2004GL021793.

Dunham, E. M. and H. S. Bhat (2008), Attenuation of radiated ground motion and stresses from three-dimensional supershear ruptures, Journal of Geophysical Research, 113, B08319, doi:10.1029/2007JB005182.

Ely, G. P., S. M. Day, and J. B. Minster (2008). A support-operator method for viscoelastic wave modeling in 3D heterogeneous media, Geophys. J. Int. , 172, doi: 10.1111/j.1365-246X.2007.03633.x, 331-344

Ely, G., S.M. Day, and J-B. Minster (2009). Dynamic rupture models for the southern San Andreas fault, *Bull. Seism. Soc. Am.*, *100* (1), 131-150, doi:10.1785/0120090187.

Harris, R. A., M. Barall, R. Archuleta, E. M. Dunham, B. Aagaard, J. P. Ampuero, H. Bhat, V. Cruz-Atienza, L. Dalguer, P. Dawson, S. Day, B. Duan, G. Ely, Y. Kaneko, Y. Kase, N. Lapusta, Y. Liu, S. Ma, D. Oglesby, K. Olsen, A. Pitarka, S. Song, and E. Templeton (2009), The SCEC/USGS dynamic earthquake-rupture code verification exercise, Seismological Research Letters, 80(1), 119-126, doi:10.1785/gssrl.80.1.119.

Mai, P.M., and G.C. Beroza (2002). A spatial random-field model to characterize complexity in earthquake slip, J. Geophys. Res., 107(B11), 2308, doi:10.1029/2001JB000588, 2002.

Olsen, K. B., R. Madariaga, and R. Archuleta (1997). Three Dimensional Dynamic Simulation of the 1992 Landers Earthquake, Science. 278, 834-838.

Olsen, K., S.M. Day, L.A. Dalguer, J. Mayhew, Y. Cui, J. Zhu, V.M. Cruz-Atienza, D. Roten, P. Maechling, T.H. Jordan, D. Okaya and A. Chourasia (2009) ShakeOut-D: Ground motion estimates using an ensemble of large earthquakes on the southern San Andreas fault with spontaneous rupture propagation, Geophys. Res. Lett., 36, L04303, doi:10.1029/2008GL036832.

Peyrat, S., K. Olsen, and R. Madariaga (2001). Dynamic modeling of the 1992 Landers earthquake, J. Geophys. Res. 106, 26,467–26,482.

Ripperger, J., J. P. Ampuero, P.M. Mai, and D. Giardini (2007). Earthquake source characteristics from dynamic rupture with constrained stochastic fault stress, J. Geophys. Res. 112: B04311, doi:10.1029/2006JB004515.

Ripperger, J.; P. M. Mai and J.-P. Ampuero (2008) Variability of near-field ground motion from dynamic earthquake rupture simulations Bull. Seism. Soc. Am., 98 (3), 1207-1228; doi:10.1785/0120070076

Sibson, R.H. (1991). Loading of faults to failure, Bull. Seismol. Soc. Am., 81, 2493-2497.